VALIDATION AND NUMERICAL CONVERGENCE OF THE HANKEL-BESSEL AND MATHIEU RIGOROUS COUPLED WAVE ANALYSIS ALGORITHMS FOR RADIALLY AND AZIMUTHALLY — INHOMOGENEOUS, ELLIPTICAL, CYLINDRICAL SYSTEMS

J. M. Jarem

Electrical and Computer Engineering Department
University of Alabama in Huntsville
Huntsville, AL 35899, USA

Abstract—A Rigorous Coupled Wave Analysis (RCWA) algorithm for electromagnetic (EM) scattering from radially and azimuthally inhomogeneous material elliptical systems based on State Variable (SV) techniques and based on circular-cylindrical Hankel-Bessel expansion modes is developed for the first time. The algorithm in conjunction with the elliptical system RCWA algorithm [1], which was based on SV techniques and Mathieu expansion modes, is used to validate and study numerical convergence of both elliptical RCWA algorithms. The formulation of the SV, Hankel-Bessel elliptical algorithm is presented. Two numerical elliptical examples are studied in detail by both algorithms, a homogeneous one which consists of three different uniform materials located in three elliptical regions and an inhomogeneous one which consists of an azimuthal, dielectric, step profile which is located between two uniform material elliptical regions. In this paper EM field scattering from a step profile which possessed a much larger dielectric step profile difference than was studied in [1] is presented. Validation and numerical convergence data of the Hankel-Bessel and the Mathieu [1] RCWA algorithm is presented for the first time, both in plot figures and in tables, when different numbers of expansion modes were used, when different number of layers were used, and when different numbers of SV harmonics were used. Validation of the RCWA algorithms was further carried out for the homogeneous case, by using Mathieu expansion modes in all regions and was carried out by using Hankel-Bessel expansion modes and Mathieu expansion modes in different regions. Validation of the Hankel-Bessel and Mathieu [1] RCWA algorithms was observed to

a high degree of accuracy. It was found for the numerical example tested, that the number of modes used in the RCWA algorithms needed to exceed a critical minimum value in order to obtain meaningful, accurate results, and after this critical number of modes was exceeded, that convergence occurred rapidly as the number of modes increased. It was also found that as the number of layers used in the algorithm increased that the numerical accuracy of the RCWA solution slowly increased.

1. INTRODUCTION

In a very recent paper [1] a spectral domain technique called Rigorous Wave Coupled Analysis (RCWA) was used to study scattering from an inhomogeneous material, elliptical cylindrical system (please see Fig. 1, this paper). The elliptical system consisted of three, different elliptical, dielectric-permeable regions, with Reg. R2 assumed to have a permittivity which was a function of radial and angular position, whereas Regs. R1 and R3 were assumed to be homogeneous materials. The EM fields of the system were assumed to excited by an elliptical surface current located in Reg. R1. The RCWA was carried out by; (1) solving Maxwell's equation in the interior region (Reg. R1) and and exterior regions (Reg. R3) of the inhomogeneous system in terms of radial and angular Mathieu functions, (2) solving Maxwell's equation (Reg. 2) in the inhomogeneous material region by using a multi-layer state variable (SV) approach, (3) matching and enforcing EM boundary conditions at the interfaces, and (4) solving the matrix equation from the previous step to determine all of the unknowns of the system. State variable equations arise from using Floquet harmonics (Fourier series) to solve Maxwell's equations in the inhomogeneous material region. In [1] two cases were considered, the first when Reg. R2 was taken to be a homogeneous material (or uniform profile) and the second when Reg. R2 was taken to a dielectric permittivity, step profile. The homogeneous case was analyzed both by using
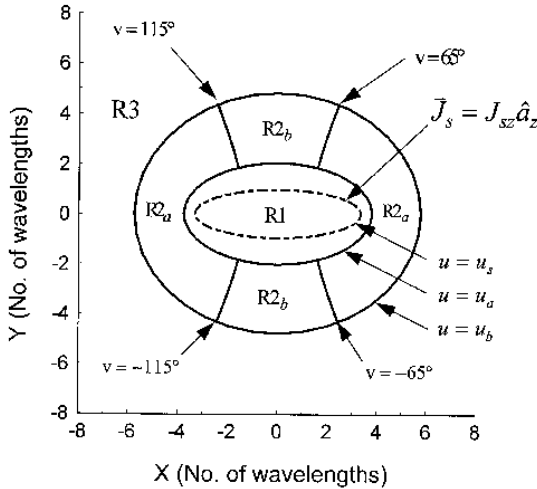
Figure 1. The geometry of the EM scattering system is shown where $\rho = 20$, $u_s = .3$, $u_a = 0.602$, and $u_b = 1.198$. For Regs. R1 and R3, $\varepsilon_1 = 1$, $\mu_1 = 1$ and $\varepsilon_3 = 1.5$, $\mu_3 = 1.2$. For the Uniform Profile case (homogeneous case) in Regs. R2$_a$ and R2$_b$, $\varepsilon_{2a} = \varepsilon_{2b} = 2.9851786$, and $\mu_{2a} = \mu_{2b} = 1.4$. For the Step Profile case (inhomogeneous case) in Regs. R2$_a$, $\varepsilon_{2a} = 2.3851786$, $\mu_{2a} = 1.4$, and in Reg. R2$_b$ is $\varepsilon_{2b} = 3.5851786$, $\mu_{2b} = 1.4$. The dielectric step difference is $\varepsilon_{2b} - \varepsilon_{2a} = 1.2$. The plot, as in [1], is drawn to exact scale.

the RCWA method and was also analyzed expanding Regs. R1, R2, and R3 in terms of radial and angular Mathieu functions and then matching boundary conditions. The RCWA and Mathieu expansion methods for the homogeneous case produced very close numerical agreement. In [1] a comparison of radial and angular Mathieu functions as obtained by solving the wave equation in elliptical coordinates and the eigenfunctions obtained by using the SV techniques for the homogeneous case were made and close agreement between the two was found.

The analysis of [1] had several limitations. The first limitation was that the analysis of [1] presented numerical results for an inhomogeneous profile example for which the change in the dielectric permittivity of the step profile in Reg. 2 was only a small amount rather than a case for which a significant dielectric step difference existed. The reason for this was that the main focus of the analysis in [1] was to compare and validate the numerical results of the homogeneous case as obtained by the RCWA method with those which were obtained by

using a Mathieu function method, rather than the study of scattering from highly inhomogeneous material. In [1] a case using only a small change in the step profile was presented mainly to illustrate the use of the RCWA method in solving inhomogeneous problems. A second limitation of [1] was that for both the homogeneous and inhomogeneous cases an analysis of the numerical convergence of the RCWA method was not carried out. A third limitation of [1] was that, except for validation of the homogeneous case by the the Mathieu expansion method, no other validation of the homogeneous or inhomogeneous cases was presented. A fourth limitation of [1] was the fact that for both the uniform and step profile cases, only a relatively small number of only propagating modes were used in the analysis. Scattering from most EM systems requires the inclusion of both propagating and evanescent (or non propagating) modes in order to meet EM boundary conditions and thus obtain a complete and correct solution.

The purpose of the present paper will be to address all four of the limitations just mentioned. These limitations will be addressed by; (1) studying an EM scattering example having a large inhomogeneity profile, (2) presentation of detailed numerical convergence of the RCWA algorithm, (3) further validation of the RCWA method, and (4) solution using a large enough number of modes to ensure that both propagating and evanescent modes are present. Concerning the first limitation, the dielectric step profile difference to be studied here will use $\varepsilon_{2b} - \varepsilon_{2a} = 1.2$ rather than $\varepsilon_{2b} - \varepsilon_{2a} = 0.1$ as was done in [1]. This example thus represents a large inhomogeneity profile. The second limitation, numerical RCWA algorithm, will be addressed by presenting numerical RCWA results as obtained when different numbers of layers are used are used in the algorithm, when different numbers of expansion modes are used in the algorithm, and when different numbers of SV harmonics are used in the algorithm.

The third limitation of [1], namely, further validation of the RCWA algorithm, will addressed by developing an RCWA algorithm which is based on using circular cylindrical, Hankel-Bessel expansion modes in Regs. R1 and R3 rather than on using Mathieu expansion modes as was done in [1]. Hankel-Bessel modes which represent solutions of the wave equation in circular cylindrical coordinates rather than in elliptical coordinates, thus will provide an independent set of basis functions (or modes) with which to expand the EM fields of the system and thus provide further validation of the algorithm. The author also believes that a RCWA algorithm which is based on using circular-cylindrical Hankel-Bessel expansion modes in Regs. R1 and R3 rather than on just Mathieu modes is a very useful one to carry out because circular-cylindrical Hankel-Bessel function modes are by

far the most common modes which are used in the solution of most cylindrical EM scattering problems.

Sec. 2 of the paper will briefly review the RCWA equations and will present the mathematical formulation of the RCWA algorithm which is based on circular cylindrical, Hankel-Bessel expansion modes in Regs. R1 and R3. Sec. 3 will present validation and numerical convergence results for both the Hankel-Bessel RCWA developed herein and the RCWA algorithm based on Mathieu functions which was developed in [1]. Sec. 4 will present summary and conclusions.

We mention in conclusion of this section, that in addition to elliptical, inhomogeneous, cylindrical systems [1], the RCWA algorithm has been applied to study EM scattering from planar diffraction grating problems [2, 3], circular cylindrical inhomogeneous problems [4, 5], bioelectromagnetic systems [6], and inhomogeneous spherical systems [7]. The textbook [8] gives a detailed description of the RCWA algorithm and gives many additional references of its application to EM scattering problems. We also mention as was done in [1], that EM scattering from elliptical systems has been carried out by many researchers, see, for example, references [9, 10]. In the present paper Mathieu function calculations have been performed based on the algorithms presented in [11, 12].

2. HANKEL-BESSEL RIGOROUS COUPLED WAVE ANALYSIS FORMULATION

As in [1] this paper is concerned with the problem of determining the EM fields that arise when an interior, elliptical surface current source (located at $u = u_s$, $u_s < u_a$) excites EM fields in an inhomogeneous, elliptical system as shown in Fig. 1. The EM analysis will be carried out by solving Maxwell's Eqs. in Regs. R1, R2, and R3 and then matching EM boundary conditions at the interfaces. It is convenient to use elliptical coordinates as specified in [11] and then normalize them. We let, $\rho = k_0 \tilde{\rho}$, $x = k_0 \tilde{x}$, $y = k_0 \tilde{y}$, $\tilde{x} = \tilde{\rho} \cosh(u) \cos(v)$, $\tilde{y} = \tilde{\rho} \sinh(u) \sin(v)$, etc. where unnormalized coordinates ($\tilde{\rho}, \tilde{x}, \tilde{y}$, etc.) are in *meters* and $k_0 = 2\pi/\lambda$ is the free space wavenumber ($1/meters$), and λ is the free space wavelength. As in [1] we assume that the system is symmetric with respect to the x and y coordinates.

The EM solution in Reg. R2 the middle inhomogeneous dielectric region is obtained [1] by dividing the dielectric Reg. R2 into N_ℓ thin elliptical shell layers of uniform value d_ℓ, $u_b - u_a = \sum_{\ell=1}^{N_\ell} d_\ell$ ($\ell = 1$ is adjacent to $u = u_b$ and $\ell = N_\ell$ is adjacent to $u = u_a$) and solve Maxwell's equations in elliptical coordinates by a state variable approach in each thin layer. Making the substitutions $U_u(u,v) =$

$\eta_0 h(u,v) H_u(u,v)$, and $U_v(u,v) = \eta_0 h(u,v) H_v(u,v)$ where $\eta_0 = 377\,\Omega$ and where $H_u(u,v)$ and $H_v(u,v)$ represent the magnetic fields in each thin shell region, letting ε and μ be respectively the relative permittivity and permeability in each thin shell region, we find that Maxwell's equations in an elliptical, cylindrical shell of coordinate value u are given by [1]

$$\frac{\partial E_z(u,v)}{\partial v} = -j\mu U_u(u,v) \tag{1}$$

$$\frac{\partial E_z(u,v)}{\partial u} = j\mu U_v(u,v) \tag{2}$$

$$\frac{\partial U_v(u,v)}{\partial u} - \frac{\partial U_u(u,v)}{\partial v} = j\varepsilon(u,v)h^2(u,v)E_z(u,v) \tag{3}$$

$$h(u,v) = \left(\rho/\sqrt{2}\right)\left[\cosh(2u) - \cos(2v)\right]^{1/2} \tag{4}$$

To solve Eqs. (1)–(4), we expand in the Floquet harmonics $0 \leq v \leq 2\pi$ [1]:

$$E_z(u,v) = \sum_{i=-\infty}^{\infty} S_{zi}(u)e^{jiv}, \qquad U_u(u,v) = \sum_{i=-\infty}^{\infty} U_{ui}(u)e^{jiv},$$

$$U_v(u,v) = \sum_{i=-\infty}^{\infty} U_{vi}(u)e^{jiv},$$

$$\varepsilon_h(u,v)E_z(u,v) = \sum_{i=-\infty}^{\infty}\left[\sum_{i'=-\infty}^{\infty} \breve{\varepsilon}_{h,i-i'}S_{zi'}\right]e^{jiv},$$

$$\varepsilon_h(u,v) \equiv \varepsilon(u,v)h^2(u,v) = \sum_{i=-\infty}^{\infty} \breve{\varepsilon}_{hi}(u)e^{jiv} \tag{5}$$

If these expansions are substituted in Eqs. (1)–(4), and after letting $\underline{S_z}(u) = [S_{zi}(u)]$, $\underline{U_u}(u) = [U_{ui}(u)]$, and $\underline{U_v}(u) = [U_{vi}(u)]$ be column matrices and $\underline{\underline{\varepsilon_h}}(u) = [\breve{\varepsilon}_{h,i-i'}(u)]$, $\underline{\underline{K}} = [iK\delta_{i,i'}]$, $K = 2\pi/\Lambda_v$, $\Lambda_v = 2\pi$ (Λ_v is the elliptical grating period and $\delta_{i,i'}$ is the Kronecker delta) be square matrices, we find after manipulation [1]

$$\frac{\partial \underline{V}}{\partial u} = \underline{\underline{A}}\,\underline{V}, \qquad \underline{V} = \left[\begin{array}{c} \underline{S_z} \\ \hline \underline{U_v} \end{array}\right], \qquad \underline{\underline{A}} = \left[\begin{array}{c|c} \underline{\underline{A_{11}}} & \underline{\underline{A_{12}}} \\ \hline \underline{\underline{A_{21}}} & \underline{\underline{A_{22}}} \end{array}\right] \tag{6}$$

where

$$\underline{\underline{A_{11}}} = 0, \qquad \underline{\underline{A_{12}}} = j\mu\underline{\underline{I}}, \qquad \underline{\underline{A_{21}}} = j\left[\underline{\underline{\varepsilon_h}} - \frac{1}{\mu}\underline{\underline{K}}^2\right], \qquad \underline{\underline{A_{22}}} = 0 \tag{7}$$

After truncating and solving the SV equations given in Eqs. (6)–(7) it is found that the EM fields in each thin layer in Reg. R2 associated with Eq. (5) are given by ([1], Eqs. (14)–(15))

$$E_{zn}(u,v) \quad = \quad E_{zn}^e(v) \exp(Q_n u) \tag{8}$$

$$E_{zn}^e(v) \quad = \quad \sum_{\substack{i=-M_T \\ (\text{even } i)}}^{M_T} S_{zin} \exp(jiv), \tag{9}$$

$$U_{vn}(u,v) \quad \equiv \quad \eta_0 h(u,v) H_{vn}(u,v) = U_{vn}^e(v) \exp(Q_n u) \tag{10}$$

$$U_{vn}^e(v) \quad = \quad \sum_{\substack{i=-M_T \\ (\text{even } i)}}^{M_T} U_{vin} \exp(jiv) \tag{11}$$

where Q_n, S_{zin}, and U_{vin} represents the eigenvalue and eigenvector coefficients of the nth mode in the lth layer in the system, and M_T represents a series truncation order. Let N_{SV} represent the number of nonzero, independent Fourier harmonics used in the state variable calculation. The SV sums in Eqs. (8)–(11) from $m = -M_T, -M_T + 2, \ldots, -2, 0, 2, \ldots, M_T - 2, M_T$ have $N_{SV} = M_T/2 + 1$ when the even symmetry of the EM fields was taken into account. By summing the eigensolutions of Eqs. (5)–(11) in each thin layer an overall solution at any point in Reg. R2 may be found. Details are given in [1].

As mentioned in the Introduction one of the purposes of the present paper is to provide an alternate formulation of the RCWA algorithm which is based on using circular-cylindrical Hankel-Bessel expansion modes in Regs. R1 and R3 rather than on using Mathieu expansion modes in Regs. R1 and R3 as was presented in [1]. Hankel-Bessel modes which represent solutions of the wave equation in circular cylindrical coordinates rather than elliptical coordinates, thus will provide an independent set of basis modes or functions with which to expand the EM fields of the system and thus provide further validation of the RCWA algorithm based on Mathieu modes which was presented in [1]. As mentioned in the Introduction Hankel-Bessel modes are the most common modes used to solve most cylindrical scattering problems.

Using circular cylindrical Hankel-Bessel expansion modes in Reg. R1 it is found that the total EM fields in Reg. R1 are given by

$$E_z^{(1)} \quad = \quad E_{z1}^I(u,v) + E_{z1}^S(u,v) \tag{12}$$

$$E_{z1}^S(u,v) \quad = \quad \sum_{m=0,2,4,\ldots}^{\infty} A_{m1} J_m(k_1 \rho_c) \cos(m\phi_c) \tag{13}$$

$$H_v^{(1)}(u,v) = H_{v1}^I(u,v) + H_{v1}^S(u,v) \tag{14}$$

$$H_{v1}^S(u,v) = \frac{1}{j\eta_0\mu_1 h(u,v)} \frac{\partial E_{z1}^S(u,v)}{\partial u} \tag{15}$$

$$\frac{\partial E_{z1}^S(u,v)}{\partial u} = \frac{\partial E_{z1}^S(u,v)}{\partial \rho_c} \frac{\partial \rho_c}{\partial u} + \frac{\partial E_{z1}^S(u,v)}{\partial \phi_c} \frac{\partial \phi_c}{\partial u} \tag{16}$$

$$\frac{\partial E_{z1}^S(u,v)}{\partial \rho_c} = \sum_{m=0,2,4,\dots}^{\infty} A_{m1} k_1 J_m'(k_1\rho_c) \cos(m\phi_c) \tag{17}$$

$$\frac{\partial E_{z1}^S(u,v)}{\partial \phi_c} = \sum_{m=0,2,4,\dots}^{\infty} A_{m1} J_m(k_1\rho_c)(-m) \sin(m\phi_c) \tag{18}$$

where $k_1 = \sqrt{\mu_1\varepsilon_1}$, the quantities $E_{z1}^I(u,v)$, $H_{v1}^I(u,v)$ represent the incident EM fields in Reg. 1 which are excited by the elliptical current source assumed to be located in an infinite uniform region whose relative permittivity and permeability value is that of Reg. R1 (please refer to [1] for details), ρ_c and ϕ_c represent radial and angular circular, cylindrical coordinates respectively, J_m refers to a Bessel function of order m, and J_m' refers to the derivative of the Bessel function of order m with respect to its argument. The incident EM fields $E_{z1}^I(u,v)$ and $H_{z1}^I(u,v)$ have been derived in [1] in terms of Mathieu function modes and the reader may refer to [1] for the equations for these quantities. The radial and angular circular, cylindrical coordinates ρ_c, ϕ_c and the ρ_c, ϕ_c partial derivatives may be expressed in elliptical coordinates as

$$\rho_c = \frac{\rho}{\sqrt{2}}[\cosh(2u) + \cos(2v)]^{1/2} \tag{19}$$

$$\frac{\partial \rho_c}{\partial u} = \frac{\rho^2}{2\rho_c} \sinh(2u) \tag{20}$$

$$\phi_c = \tan^{-1}[\tanh(u)\tan(v)] \tag{21}$$

$$\frac{\partial \phi_c}{\partial u} = \frac{\tan(v)}{\cosh^2(u) + \sinh^2(u)\tan^2(v)} \tag{22}$$

In Reg. R3 using outgoing circular, cylindrical Hankel functions which satisfy the wave equation in circular, cylindrical coordinates it is found that the total EM fields are given by

$$E_z^{(3)}(u,v) = \sum_{m=0.2,4,\dots}^{\infty} A_{m3} H_m^{(2)}(k_3\rho_c) \cos(m\phi_c) \tag{23}$$

$$H_v^{(3)}(u,v) = \frac{1}{j\eta_0\mu_3 h(u,v)} \frac{\partial E_z^{(3)}(u,v)}{\partial u} \tag{24}$$

$$\frac{\partial E_z^{(3)}(u,v)}{\partial u} = \sum_{m=0,2,\ldots}^{\infty} A_{m3} \left[k_3 H_m^{(2)\prime}(k_3\rho_c) \cos(m\phi_c) \frac{\partial \rho_c}{\partial u} \right.$$

$$\left. + H_m^{(2)}(k_3\rho_c)(-m)\sin(m\phi_c)\frac{\partial \phi_c}{\partial u} \right] \qquad (25)$$

where $k_3 = \sqrt{\mu_3 \varepsilon_3}$, $H_m^{(2)}$ refers to a Hankel function of the second kind (outgoing) of order m and $H_m^{(2)\prime}$ refers to a derivative with respect to its argument of a Hankel function of order m of the second kind.

Now that the general form of the EM fields have been specified in all regions, the next step in analysis is to match the tangential EM fields at all interfaces of the system and determine all the unknowns in the system. In this paper and in [1] the boundary matching step has been carried out by; (1) equating the appropriate tangential electric and magnetic field expansions as defined by Eqs. (1)–(25) at each interface, (2) multiplying the resulting equations (both electric and magnetic) by an electric field expansion function (also called a testing, weighting, or enforcing function) which exists in a layer which is adjacent to the interface, and (3) integrating the resulting equations over the azimuthal elliptical region $0 \le v \le 2\pi$ (the radial angular elliptical variable u is constant over this interval). When an RCWA solution is being implemented the electric field testing expansion or testing function used in this paper and [1] are the thin layer, eigenmode (or eigenfunction) solutions of the SV equations of Reg. R2 defined in Eqs. (8)–(11). Using the above procedure a matrix equation for the overall system is formed and solved, and all of the unknowns of the system are determined. Ref. [1] gives a detailed description of the procedure which has just been described.

In addition to the RCWA solution presented here, two alternate expansion mode methods have been developed to determine the elliptical scattering problem for the homogeneous case. The first method which was presented in [1] was based on using Mathieu expansion modes in Regs. R1, R2, and R3 to expand the unknown EM fields of the homogeneous system, and from these expansions, after imposing boundary conditions, solving a matrix equation for the unknowns of the system. The second expansion method which is being implemented in this paper for the first time, is same as the first, except that circular-cylindrical Hankel-Bessel modes are used in Regs. R1 and R3 to expand the EM fields of the homogeneous system rather than Mathieu function modes in Regs. R1 and R3 as was done in [1]. In both of these methods, Mathieu function modes are used as testing modes to form a matrix equation from which all of the unknowns of the system are determined. The Mathieu mode and Hankel-Bessel

mode expansion methods, which only apply to the homogeneous case, have been developed in order to provide additional and independent ways of validating the RCWA solutions.

3. NUMERICAL RESULTS

This section will present numerical convergence and validation results for the RCWA algorithms. Two numerical examples or cases are studied in detail by both algorithms, namely, a homogenous case which consists of three different uniform materials located in three elliptical regions and an inhomogeneous case which consists of an azimuthal dielectric step-profile which is located between two uniform material elliptical regions (please see Fig. 1). In this paper (and [1]) the elliptic parameter $\rho = k_0 \tilde{\rho}$ was taken to have a value $\rho = 20$, the inner Reg. R1-R2 interface was taken to have a value $u = u_a = .602$, and the outer Reg. R2-R3 boundary was taken to have a value $u = u_b = 1.198$. (In elliptic coordinates, $x = k_0 \tilde{x} = \rho \cosh(u) \cos(v)$, $y = k_0 \tilde{y} = \rho \sinh(u) \sin(v)$, where $k_0 = 2\pi/\lambda$.) The material values of the relative dielectric permittivity and permeability for both the homogeneous case and inhomogeneous case (please see Fig. 1) in Regs. R1 and R3 respectively, are $\varepsilon_1 = 1$, $\mu_1 = 1$ and $\varepsilon_3 = 1.5$, $\mu_3 = 1.2$. For the homogeneous case in Reg. R2 the relative permittivity and permeability values in Regs. R2$_a$ and R2$_b$ are $\varepsilon_{2a} = \varepsilon_{2b} = 2.9851786$, $\mu_{2a} = \mu_{2b} = 1.4$. For the inhomogeneous case in Reg. R2 the relative permittivity and permeability values in Reg. R2$_a$ is $\varepsilon_{2a} = 2.3851786$, $\mu_{2a} = 1.4$ and in Reg. R2$_b$ is $\varepsilon_{2b} = 3.5851786$, $\mu_{2b} = 1.4$. Electromagnetic fields are excited in the overall system by an elliptical surface current source which was located at $u = u_s = .3$, $\rho = 20$ (please see Fig. 1). This source (which is assumed nonuniform in the angular v direction and is the same one as used in [1]) was chosen to excite a $m = 0$ Mathieu mode when it is located in an infinite uniform region whose relative permittivity and permeability value is that of Reg. R1. Ref [1] gives the details of this source. The total, unnormalized power per unit length radiated from the elliptical surface current source used in this paper and in [1] ($\vec{J}_S(u_s, v)$ of Eq. (35) of [1]) when Reg. R1 is infinite and $\varepsilon_1 = 1.$, $\mu_1 = 1.$ is $P_{JS} = 6.816674 \times 10^{-2}/377 = 1.80813634 \times 10^{-4}$ (Watts/m). (In [1] P_{JS} was misreported as $P_{JS} = 6.816674 \times 10^{-2}$ (Watts/m) or was reported *before* division by 377. The normalized power ratio $P_{NOR} = P_{TOT}/P_{JS}$ of Table 1 and Fig. 8 specified in [1] has been correctly reported.)

The inhomogeneous example chosen here uses the same geometry, material constants, and excitation as was used in [1], except for the

very important difference that a large, dielectric-step, difference profile is used here ($\varepsilon_{2b} = 3.5851786$, $\varepsilon_{2a} = 2.3851786$, or $\varepsilon_{2b} - \varepsilon_{2a} = 1.2$) whereas in [1] a small one was used ($\varepsilon_{2b} = 3.05$, $\varepsilon_{2a} = 2.95$, or $\varepsilon_{2b} - \varepsilon_{2a} = 0.1$). In [1] and in the present paper, a step profile example has been chosen to represent a dielectric inhomogeneity profile because a step profile possesses a high azimuthal spectral content (being a step function) and thus represents a good test of the RCWA algorithms since many higher order harmonics must be included in the analysis for accurate numerical results. As in [1] the step profile and the current source excite are symmetric in the four quadrants of the xy plane and thus excite an E_z electric field and an H_v magnetic field which is also symmetric in both the x and y coordinates. The homogeneous case for which numerical convergence and validation data will be presented herein is the same case as was studied in [1].

At this point we would now like to discuss the determination, labeling, and ordering of the SV modes which were used to study the step profile case under consideration. The SV modes corresponding to the step profile case have been determined by; (1) initially, solving for the SV modes of the homogenous case using SV techniques (the SV solutions are Mathieu modes corresponding to orders $m = 0, 2, 4, \ldots$); (2) increasing, by a small increment, the dielectric step profile difference between Regs. R2$_b$ and R2$_a$; (3) solving the SV equations for new eigenvalues for the new step profile difference of Step (2); and (4) repeating Steps (1)–(3) many times, using each time the new SV modes from Steps (2) and (3) as the new initialization for Step (1), until the dielectric step profile difference reached is the final value desired, which in this case would be $\varepsilon_{2b} - \varepsilon_{2a} = 1.2$. By following this procedure in each thin layer for each mode, it was possible to see a continuous change of the eigenvalue of a given mode from its value when it corresponded to the homogeneous case (a Mathieu mode value) to its final value when $\varepsilon_{2b} - \varepsilon_{2a} = 1.2$. The change of the eigenvalue with dielectric step profile difference may be called an eigenvalue mode branch. The inhomogeneous modes used in this paper were labeled by associating each eigenvalue mode branch with the Mathieu mode order which occurred at the start of the branch when the Reg. R2 was uniform (or homogeneous). Thus $m = 0, 2, 4, \ldots$ Mathieu modes corresponded to $n = 1, 2, 3, \ldots$ Step Profile SV modes. In making the mode branch association, it was checked that outgoing Mathieu modes corresponded to outgoing SV modes and that incoming Mathieu modes corresponded to incoming SV modes. It was not necessary to carry out this procedure in [1], since only a small value of the dielectric step profile difference and a small number of modes were used, and thus the system eigenmodes did not differ greatly from the Mathieu modes of
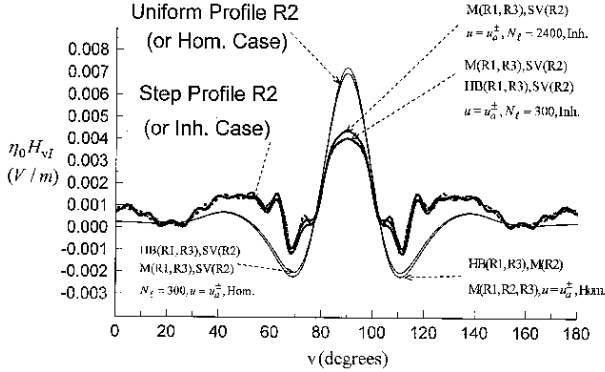
Figure 2. Plots of $\eta_0 H_{vI}$ where H_{vI} is the imaginary part of the magnetic field H_v are shown for the Uniform Profile R2 and Step Profile R2 cases (see Fig. 1). The light solid lines, labeled Uniform Profile R2 (eight plots total) have been computed numerically at $u = u_a^\pm$ using the expansion mode sets which are labeled on the figure. The heavy solid and dashed lines, labeled Step Profile R2 (six plots total), have been computed numerically at $u = u_a^\pm$ using the expansion mode sets which are labeled on the figure. All expansion mode sets used 30 modes.

the homogeneous case.

In carrying out this procedure for the step profile case ($\varepsilon_{2b} - \varepsilon_{2a} = 1.2$) for the thin layer in Reg. R2 which was adjacent to the $u = u_a$ boundary (or Reg. R1-R2 interface), using a SV analysis involving 54 harmonics ($N_{SV} = 54$) to determine the first 30 modes (with the mode orders labeled as described earlier), it was observed that the first 19 outgoing SV modes were propagating (i.e., Q_n in Eq. (8) had an imaginary, negative value) and that the next 11 outgoing SV modes were evanescent (i.e., Q_n in Eq. (8) had a real, negative value). A similar observation was made for the SV incoming modes in this thin layer. It was also observed for the same step profile case ($\varepsilon_{2b} - \varepsilon_{2a} = 1.2$), that in the thin layer in Reg. R2 which was adjacent to the $u = u_b$ (or Reg. R2-R3 interface), that all 30 of the outgoing SV modes or incoming SV modes were propagating. It is thus seen for the present step profile numerical example ($\varepsilon_{2b} - \varepsilon_{2a} = 1.2$), that both propagating and evanescent modes play a role in determining the final EM fields of the system. One also sees for the present example, that out of the thirty modes, that as one moves radially outward from one thin layer to another, that gradually less modes are evanescent and more modes become propagating.

We will now present plots in Figs. 2–8 of the EM fields as

calculated by the Hankel-Bessel and Mathieu RCWA algorithms for the Uniform Profile case (or homogeneous case) and Step Profile case (or inhomogeneous case) which have been discussed earlier. Fig. 1 shows the geometry of the scattering system. Thirty expansion modes in each region were used to make all the plots to be shown in Figs. 2–8. By 30 expansion modes, it is meant that 30 outgoing expansion modes were used in Reg. R3, 30 outgoing modes and 30 incoming expansion modes were used in Reg. R2, and that 30 expansion modes in Reg. R1 which are finite at the origin were used.

Fig. 2 shows plots of $\eta_0 H_{vI}$ where H_{vI} is the imaginary part of the magnetic field H_v. In Fig. 2 H_{vI} is evaluated at the inner boundary $u = u_a^-$ (Reg. 1 side) and is evaluated at the inner boundary $u = u_a^+$ (Reg. 2 side). H_{vI} has been calculated at $u = u_a^\pm$ in the cases when a homogeneous elliptical profile (homogeneous case) is present in Reg. R2 and in the case when a step profile (inhomogeneous case) is present in Reg. R2. As can be seen from Fig. 2, quite different plots results occur for uniform or step profile cases. The plots of Fig. 2 for the homogeneous case (all *light solid line*, labeled *Uniform Profile* (*or Homogeneous Case*), eight plots total) have been computed numerically at $u = u_a^-$, (Reg. R1 side) and $u = u_a^+$ (Reg. R2 side) by using four different combinations of expansion modes in the different regions, namely; (1) M(R1,R2,R3); (2) HB(R1,R3),M(R2); (3) M(R1,R3),SV(R2), $N_\ell = 300$; and (4) HB(R1,R3),SV(R2), $N_\ell = 300$; where M refers to Mathieu modes, HB refers to Hankel-Bessel modes, SV refers to State Variable modes, R1,R2, or R3 refers to the region where the expansion mode was used, and N_ℓ refers to number of layers used in the SV expansion method. The third and fourth expansion sets represent the Mathieu and Hankel-Bessel RCWA algorithms respectively. As can be seen from Fig. 2, the four different sets of expansion modes for the homogeneous case all produce numerical results which are very close to each other. Boundary matching at $u = u_a^\pm$, using the four different expansion mode sets, produced such close results that the plots for each expansion set, evaluated on the at $u = u_a^-$ (Reg. R1 side) and on the $u = u_a^+$ (Reg. R2 side), could not be separated from one another. The homogeneous case plots (*light solid line*) which have a slightly larger peak value, corresponded to the two expansion sets which used Mathieu modes in Reg. R2 (namely, M(R1,R2,R3) and HB(R1,R3),M(R2)), whereas the plots (*light solid line*) which have the slightly lower peak values lower, corresponded to the two expansion sets which used the Mathieu and Hankel-Bessel RCWA algorithms (namely, M(R1,R3),SV(R2), $N_\ell = 300$ and HB(R1,R3),SV(R2), $N_\ell = 300$). Overall it is felt that the homogeneous case plots of Fig. 2 provide a good validation that

the RCWA algorithms are working correctly.

The plots of Fig. 2 for the inhomogeneous case (*heavy solid and dashed lines*, labeled *Step Profile* (*or Inh. Case*), six plots total) have been computed numerically at $u = u_a^-$ (Reg. R1 side) and $u = u_a^+$ (Reg. R2 side) by using; (1) the Mathieu RCWA algorithm M(R1,R3),SV(R2) with $N_\ell = 2400$ (2 *heavy solid lines*), (2) the Mathieu RCWA algorithm M(R1,R3),SV(R2) with $N_\ell = 300$ (2 *heavy solid lines*), and (3) the Hankel-Bessel RCWA algorithm HB(R1,R3),SV(R2) with $N_\ell = 300$ (2 *heavy dashed lines*). We remind the reader the first two expansion sets (M(R1,R2,R3) and HB(R1,R3),M(R2)) used for the homogeneous case cannot be used to determine the EM fields for the step profile case because Mathieu modes in Reg. R2 do not represent modal solutions of Maxwell's Equations. As can be seen from the Fig. 2 step profile plots, the Mathieu and Hankel-Bessel RCWA algorithms produce results which are all fairly close to each other. As in the homogeneous case, boundary matching at $u = u_a^\pm$ using; (1) M(R1,R3),SV(R2), $N_\ell = 2400$, (2) M(R1,R3),SV(R2), $N_\ell = 300$, or (3) M(R1,R3),SV(R2), $N_\ell = 300$, each produced such close boundary matching results that the plots for each case evaluated on the $u = u_a^-$ (Reg. R1 side) and on the $u = u_a^+$ (Reg. R2 side), could not be distinguished from one another. As can be seen from Fig. 2, step profile plots using the Hankel-Bessel and Mathieu RCWA algorithms using the same number of layers $N_\ell = 300$, produced close numerical results to each other. Also, as can be seen from the Fig. 2 plots, the number of layers N_ℓ used did made a small difference in the numerical results for the for the inhomogeneous case. The plots of the Mathieu RCWA algorithm M(R1,R3),SV(R2) using $N_\ell = 2400$ layers, which must be considered the most accurate RCWA calculation of the three RCWA step profile calculations presented, had a slightly higher peak value than those of the other two which used $N_\ell = 300$. Overall all three expansion sets produced very similar numerical results.

Fig. 3 shows plots of the real part of the electric field E_z, namely E_{zR}, when it is evaluated at the outer boundary at $u = u_b^-$ (Reg. R2 side) and when it is evaluated at the outer boundary at $u = u_b^+$ (Reg. R3 side). The plots of Fig. 3 were calculated for the same numerical cases and the same expansion mode sets as were described in Fig. 2. As can be seen from Fig. 3 excellent agreement of numerical results occurred between all the expansion sets for the homogeneous case and for the inhomogeneous case being considered. As in Fig. 2 it is observed that for the homogeneous plots, that the M(R1,R2,R3) and HB(R1,R3),M(R2) expansion sets correspond to peak to peak values which were slightly greater than the RCWA expansion sets
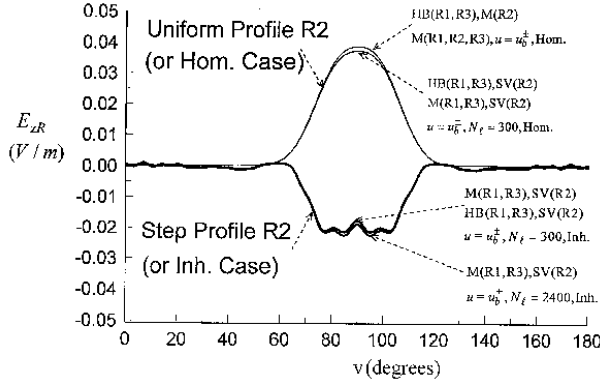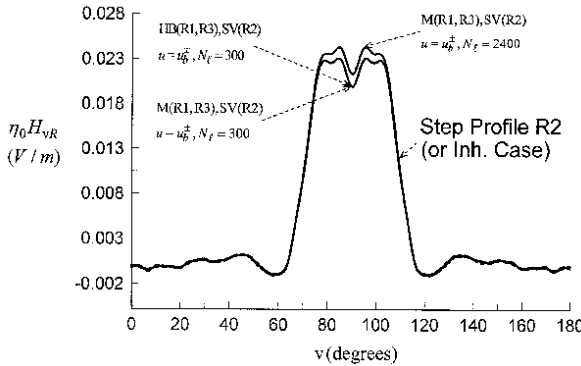
Figure 3. Plots of E_{zR} where E_{zR} is the real part of the electric field E_z are shown for the Uniform Profile R2 case and shown for the Step Profile R2 case as calculated at $u = u_b^{\pm}$ (see Fig. 1). The plots are calculated by the same expansion mode sets as were used in Fig. 2.

M(R1,R3),SV(R2), $N_\ell = 300$ and HB(R1,R3),SV(R2), $N_\ell = 300$, respectively. Overall it is felt, that as in plots of Fig. 2, that the homogeneous plots of Fig. 3 for E_{zR} provide a good validation that the RCWA algorithms are working correctly. It is also observed for the inhomogeneous plots (*heavy lines*) in Fig. 3, that the number of layers N_ℓ used did made a small difference in the numerical results for this case. The Mathieu RCWA plots for M(R1,R3),SV(R2), $N_\ell = 2400$, which as in Fig. 2 must be considered the most accurate, had a slightly lower value than those of the other two sets which used $N_\ell = 300$. It is interesting to note in Fig. 3, that when comparing the homogeneous and inhomogeneous cases, that the real parts of the electric field for the homogeneous case is nearly positive or zero for most values of coordinate v, whereas of the electric field for the inhomogeneous case is nearly negative or zero for most values of v. This is most likely caused by the fact that the optical path length from $u = u_a$ to $u = u_b$ in the step profile case is different from the optical path length in the uniform profile case, thus causing a sign difference between the two cases. As in Fig. 2, boundary matching in Fig. 3 at $u = u_b^{\pm}$ for the homogeneous and inhomogeneous cases for each expansion set was so close that the difference on the two sides of boundary could not be observed in the plots.

Figs. 4, 5, and 6 show respectively, E_{zI} the imaginary part of the electric field, and the real and imaginary parts of the field $\eta_0 H_v$ as evaluated at $u = u_b^{\pm}$. In these plots only the step profile (or inhomogeneous case) numerical results are presented. The plots of
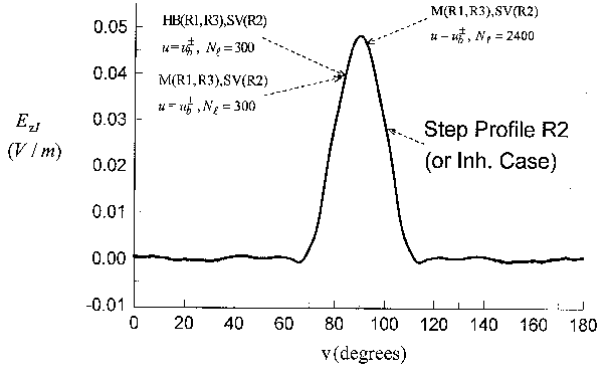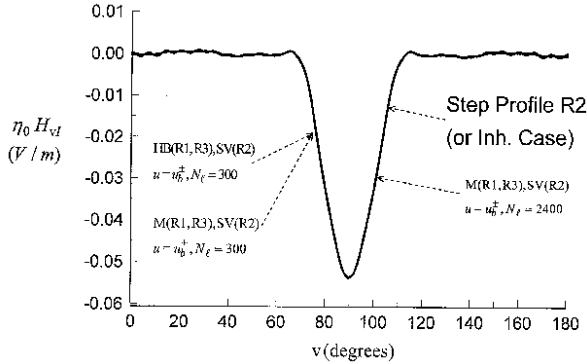
Figure 4. Plots of E_{zI} where E_{zI} is the imaginary part of the electric field E_z are shown for the Step Profile R2 case as calculated at $u = u_b^{\pm}$ (see Fig. 1). The plots are calculated by the same expansion mode sets as were used in Fig. 2 for the Step Profile.


Figure 5. Plots of $\eta_0 H_{vR}$ where $\eta_0 H_{vR}$ is the real part of the magnetic field H_v are shown for the Step Profile R2 case as calculated at $u = u_b^{\pm}$ (see Fig. 1). The plots are calculated by the same expansion mode sets as were used in Fig. 2 for the Step Profile.

Figs. 4, 5, and 6 were calculated for the same inhomogeneous case and the same expansion function sets as were described in Figs. 2 and 3. In observing Figs. 4, 5, and 6 it is interesting to note that in Figs. 4 and 6 that the number of layers made almost no difference in the numerical results displayed, but that in Fig. 5 a slight difference in the numerical results with layer number was observed. Overall in Figs. 4–6, as in Figs. 2 and 3, it is felt that all three expansion sets produced very similar numerical results.

Figure 6. Plots of $\eta_0 H_{vI}$ where $\eta_0 H_{vI}$ is the imaginary part of the magnetic field H_v are shown for the Step Profile R2 case as calculated at $u = u_b^{\pm}$ (see Fig. 1). The plots are calculated by the same expansion mode sets as were used in Fig. 2 for the Step Profile.

Figs. 7 and 8 show, respectively, a three dimensional plot of the E_{zR} field for the uniform profile case and a three dimensional plot of the E_{zR} field for the step profile case, versus the normalized rectangular coordinates $X = \tilde{x}/\lambda$, $Y = \tilde{y}/\lambda$, where λ is the free space wavelength. The three dimension figures were plotted over the first quadrant of the XY plane and were calculated by using the Mathieu RCWA algorithm M(R1,R3),SV(R2) using 300 layers and 30 modes. Because the electric field is symmetric in the XY coordinates, only one quadrant has been displayed. In Figs. 7 and 8, the dotted curves labeled $u = u_a$ and $u = u_b$ shows, respectively, the Reg. R1-R2 and Reg. R2-R3 boundaries in the XY plane of the elliptical system. In comparing the plots of Fig. 7 (uniform profile, Reg. R2 (or homogeneous case)) and Fig. 8 (step profile, Reg. R2 (or inhomogeneous case)), the first feature that one notices immediately, is that in Fig. 8 (step profile), in all elliptical Regs. R1,R2,R3 (and particularly Reg. R1), that the electric field E_{zR} shows a high degree of interference in the angular (or azimuthal) v direction, whereas in Fig. 7 (uniform profile) that there is almost no interference in this direction. This is a very believable result since one would expect in the step profile case (Fig. 8) that the incident EM fields would be highly scattered by the step profile discontinuity and the resulting scattered fields would then be multiply reflected in the overall system, causing a complicated interference pattern in the angular v direction. This is exactly what is seen in Fig. 8. When viewing Figs. 7 and 8, it is further observed in both figures, that the E_{zR} field component is continuous at all material boundaries and thus
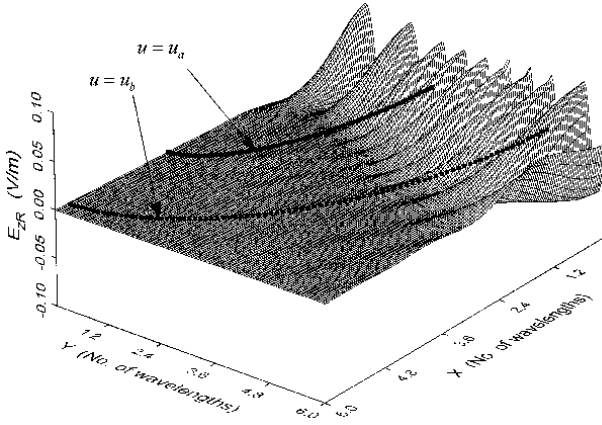
Figure 7. A plot of the real electric field E_{zR} (over the first quadrant of Fig. 1) as resulted for the Uniform Profile R2 case (homogeneous case) versus the normalized rectangular coordinates $X = \tilde{x}/\lambda$, $Y = \tilde{y}/\lambda$, (λ is the free space wavelength) is shown. The dotted curves labeled $u = u_a$ and $u = u_b$ shows respectively the Reg. R1-R2 and Reg. R2-R3 boundaries (see Fig. 1). The plot was made using 30 modes of the expansion set M(R1,R3),SV(R2) and using $N_\lambda = 300$ layers.
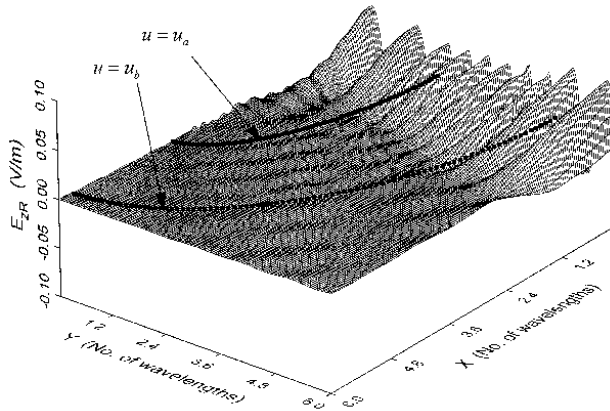
Figure 8. A plot of the real electric field E_{zR} (over the first quadrant of Fig. 1) as resulted for the Step Profile R2 case (inhomogeneous case) versus the normalized rectangular coordinates $X = \tilde{x}/\lambda$, $Y = \tilde{y}/\lambda$, is shown. The plot was made using 30 modes of the expansion set M(R1,R3),SV(R2) and using $N_\lambda = 300$ layers.

satisfies proper the EM boundary conditions as it must in order to be a valid EM solution. When viewing Figs. 7 and 8, it is further observed that the approximate separation of the peaks of the E_{zR} field, as observed in the different material regions is, either is smaller or larger according to whether the material's index of refraction ($\sqrt{\mu\varepsilon}$) in that region (please see Fig. 1) is either *larger* or *smaller* as one would expect of a correct EM field solution. This is clearly seen, for example, in both Figs. 7 and 8 when comparing the field in Reg. R1 with the E_{zR} field in Reg. R2.

Tables 1 and 2, respectively, display the normalized power for the homogeneous and inhomogeneous cases which is radiated through the interfaces $u = u_a^-$, $u = u_a^+$, $u = u_b^-$, and $u = u_b^+$, when four different expansion mode sets are used (described earlier for Fig. 2), when a different numbers of modes are used, when a different number of state variable harmonics are used, and when a different number of layers, N_ℓ are used. The normalized power through a fixed u interface, is found by integrating the real time averaged power (as calculated by using the Poynting vector) over the interval $0 \le v \le 2\pi$ and then dividing this quantity by the power which is radiated by the elliptical current source when the elliptical current source is an infinite uniform region having material constants equal to those of Reg. R1. The '# Modes' in Tables 1 and 2 means the number of outgoing expansion modes that were used in Reg. R3, the number of outgoing and the number of incoming expansion modes that were used in Reg. R2, and the number of expansion modes which are finite at the origin that were used in Reg. R1. The number of '# SV Harmonics' in Table 2 means the number of nonzero, independent harmonics that were used to make the calculation, namely, N_{SV} ($N_{SV} = \frac{M_T}{2} + 1$ for Eqs. (8)–(11)). All SV calculations in Table 1 used $N_{SV} = 54$ state variable harmonics in region R2.

In the first set of data presented in Table 1 (uniform profile case, Reg. R2 (or homogeneous case)) 1,2,5,10,15 and 30 (Mathieu modes have been used in Regs. R1, R2, and R3 to calculate the normalized power. As one can observe, when only one mode (the $m = 0$ mode) is used, different values of the normalized power as calculated at the interfaces $u = u_a^-$, $u = u_a^+$, $u = u_b^-$, and $u = u_b^+$ occurs. As the number of modes used increases, however, the normalized power as calculated at the interfaces $u = u_a^-$, $u = u_a^+$, $u = u_b^-$, and $u = u_b^+$ become increasingly close to one another. The normalized power results for the cases when 15 and 30 modes were used, were very close to each other and to all being the same value. In the second set of data of Table 1, 30 Hankel-Bessel expansion modes were used in Regs. R1 and R3 and 30 Mathieu modes were used in Reg. R2.

Table 1. Numerical values of the normalized power for the Uniform Profile R2 case (see Fig. 1) which is radiated through the interfaces $u = u_a^-$, $u = u_a^+$, $u = u_b^-$, and $u = u_b^+$, when four different expansion mode sets are used, when a different numbers of modes are used, and when a different number of layers $N_\ell = 300$ are used are displayed. All normalized power results in Table 1 used 54 state variable harmonics. By '# modes', it is meant the number of outgoing modes in Reg. R3, the number of outgoing mode or incoming modes in ReG. R2, and the number of modes in Reg. R1 which are finite at the origin.

Expansion Modes (M=Mathieu, HB=Hankel-Bessel, SV=State Variable)	# Modes (Regs. R1,R2, or R3)	# Layers (Reg.R2)	P_{NOR} $u = u_a^-$, Reg. R1	P_{NOR} $u = u_a^+$, Reg. R2	P_{NOR} $u = u_b^-$, Reg. R2	P_{NOR} $u = u_b^+$, Reg. R3
M(R1,R2,R3)	1	1	0.7165889	0.6719399	0.6719399	0.6872527
M R1,R2,R3)	2	1	0.7280368	0.7270724	0.7270724	0.7295875
M(R1,R2,R3)	5	1	0.7270355	0.7270554	0.7270554	0.7271340
M(R1,R2,R3)	15	1	0.7270297	0.7270297	0.7270297	0.7270342
M(R1,R2,R3)	30	1	0.7270299	0.7270299	0.7270299	0.7270299
HB(R1,R3), M(R2)	30	1	0.7270299	0.7270299	0.7270299	0.7270299
M(R1,R3), SV(R2)	1	300	0.7063294	0.6623197	0.6623197	0.6774132
M(R1,R3), SV(R2)	2	300	0.7181911	0.7172787	0.7172787	0.7197630
M(R1,R3), SV(R2)	5	300	0.7171901	0.7172147	0.7172147	0.7172994
M(R1,R3), SV(R2)	15	300	0.7172154	0.7172155	0.7172155	0.7172204
M(R1,R3), SV(R2)	30	300	0.7172155	0.7172155	0.7172155	0.7172155
HB(R1,R3),SV(R2)	30	300	0.7172155	0.7172155	0.7172155	0.7172155
M(R1,R3), SV(R2)	30	150	0.7073473	0.7073473	0.7073473	0.7073473
M(R1,R3), SV(R2)	30	300	0.7172155	0.7172155	0.7172155	0.7172155
M(R1,R3), SV(R2)	30	600	0.7221315	0.7221315	0.7221315	0.7221315
M(R1,R3), SV(R2)	30	1200	0.7245831	0.7245831	0.7245831	0.7245831

As can be seen, identical normalized power results occurred (for the number of significant figures shown) as when 30 Mathieu modes were used in all regions. The next set of data used the Mathieu RCWA algorithm (M(R1,R3),SV(R2)) calculated using 1,2,5,15,30 modes and using 300 layers ($N_\ell = 300$). As in the first set of data, presented, inaccurate power matching results occurred when only one mode was used, but as the number of modes were increased, the power matching accuracy increased. The normalized power results for the cases when 15 and 30 modes were very close to being the same. In the fourth

Table 2. Numerical values of the normalized power for the Step Profile R2 case (see Fig. 1) which is radiated through the interfaces $u = u_a^-$, $u = u_a^+$, $u = u_b^-$, and $u = u_b^+$, when two different expansion mode sets are used, when a different numbers of modes are used, and when a different number of state variable harmonics are used, and when a different number of layers are used are displayed. The same designations as Table 1 are used.

Expansion Modes (M=Mathieu, HB=Hankel-Bessel, SV=State Variable)	# Modes (Regs. R1,R2, or R3)	# Layers, # SV Harmonics (Reg. R2)	P_{NOR} $u = u_a^-$, Reg. R1	P_{NOR} $u = u_a^+$, Reg. R2	P_{NOR} $u = u_b^-$, Reg. R2	P_{NOR} $u = u_b^+$, Reg. R3
M(R1,R3), SV(R2)	20	300, 32	0.5539280	0.5539239	0.5539240	0.5714681
M(R1,R3), SV(R2)	20	300, 54	0.5539233	0.5539178	0.5539178	0.5746453
M(R1,R3), SV(R2)	25	300, 54	0.5539178	0.5539272	0.5539272	0.5569690
M(R1,R3), SV(R2)	30	300, 54	0.5539072	0.5539060	0.5539060	0.5539060
M(R1,R3), SV(R2)	35	300, 54	0.5539064	0.5539057	0.5539057	0.5539059
HB(R1,R3),SV(R2)	20	300, 54	0.5539280	0.5539239	0.5539240	0.5773110
HB(R1,R3),SV(R2)	25	300, 54	0.5539181	0.5539159	0.5539159	0.5539178
HB(R1,R3),SV(R2)	30	300, 54	0.5539169	0.5539159	0.5539159	0.5539163
M(R1,R3), SV(R2)	30	150, 54	0.5442774	0.5442761	0.5442761	0.5442760
M(R1,R3), SV(R2)	30	300, 54	0.5539072	0.5539060	0.5539060	0.5539060
M(R1,R3), SV(R2)	30	600, 54	0.5588399	0.5588386	0.5588386	0.5588387
M(R1,R3), SV(R2)	30	1200, 54	0.5613346	0.5613333	0.5613333	0.5613334
M(R1,R3), SV(R2)	30	1200, 107	0.5613340	0.5613326	0.5613326	0.5613327
M(R1,R3), SV(R2)	30	2400, 54	0.5625889	0.5625877	0.5625877	0.5625878

set of data normalized power data calculated using the Hankel-Bessel RCWA algorithm (HB(R1,R3),SV(R2)) with 30 modes and using 300 layers ($N_\ell = 300$) was presented. As can be seen, identical results occurred using 30 modes of either the Hankel-Bessel or Mathieu RCWA algorithms. In the fifth set of data normalized power data calculated using the Mathieu RCWA algorithm (M(R1,R3),SV(R2)) with 30 modes and using $N_\ell = 150, 300, 600, 1200$ layers was presented. As can be seen for a given number of layers, power matching at the interfaces $u = u_a^-$, $u = u_a^+$, $u = u_b^-$, and $u = u_b^+$ agrees exactly (to the number of places shown), but, as the number of layers increases, the normalized power changes value and approaches the 30 mode values of the first and second normalized power data sets, respectively, namely, M(R1,R2,R3) and HB(R1,R3),M(R2). We mention now that the 30 mode values of the first and second data sets, respectively, M(R1,R2,R3) and HB(R1,R3),M(R2), must be regarded as the most

rigorously correct normalized power values of all of the homogeneous case calculations since they use the largest mode sets, satisfies power conservation most accurately, and are based on modal solutions in Regs. R1,R2 , and R3 which are exact solutions of the wave equation in all regions. Thus the fifth data set shows that as the number of layers is increased, convergence of the RCWA Mathieu solution to the correct solution is occurring. It is noticed in Table 1, overall, that the number of layers N_ℓ is the most sensitive parameter as to establishing an accurate solution.

In the first set of data presented in Table 2 (step profile case, Reg. R2 (or inhomogeneous case)) 20,25,30, and 35 expansion modes (M(R1,R3),SV(R2)) have been used to calculate the normalized power using $N_\ell = 300$ layers in Reg. R2. For this set of data, the number of SV harmonics, N_{SV}, was taken to be either $N_{SV} = 32$ for the 20 mode case or $N_{SV} = 54$ for the 25, 30 and 35 mode cases. We first observe for the 20 modes case that the use of $N_{SV} = 32$ or $N_{SV} = 54$ SV harmonics produced very close normalized power results to each other. We also observed from the 20 modes case (using either 32 or 54 SV harmonics) that a small error in power matching occurs between the normalized power as seen at the interfaces $u = u_a^-$, $u = u_a^+$, and $u = u_b^-$ and as seen at the $u = u_b^+$ interface. Continuing inspection of the first set of data of Table 2, we see that as the number of modes used increases, however, the normalized power as calculated at the interfaces $u = u_a^-$, $u = u_a^+$, $u = u_b^-$, and $u = u_b^+$ become increasingly close to one another. The normalized power results for 25, 30, and 35 mode cases all obeyed power conservation at the interfaces $u = u_a^-$, $u = u_a^+$, $u = u_b^-$, and $u = u_b^+$ well and were all were very close to each other in value. In the second set of data of Table 2, 20, 25, and 30 Hankel-Bessel, state variable (HB(R1,R3), SV(R2)) expansion modes were used to compute normalized power results using $N_\ell = 300$ layers and $N_{SV} = 54$ SV harmonics. As can be seen, the normalized power results for these 20, 25, and 30 mode HB(R1,R3), SV(R2) cases was very close, respectively, to the 20,25, and 30 mode M(R1,R3), SV(R2) cases presented in the first data set. As in the first data power, the normalized power results for 25 and 30 mode cases all obeyed power conservation at the interfaces $u = u_a^-$, $u = u_a^+$, $u = u_b^-$, and $u = u_b^+$ well and were all were very close to each other in value. In computing the first and second sets of data for Table 2, it was found for the step profile numerical example tested, that the number of modes used in the Mathieu or in the Hankel-Bessel RCWA algorithms needed to exceed a critical minimum value (in Table 2 about 18 to 20 modes) in order to obtain meaningful and accurate results. For 14 to 16 modes, for example (data not shown), highly incorrect and ill-conditioned numerical results

occurred. It was further found that once this critical minimum number of modes was exceeded, that the RCWA converged quickly to an accurate solution. In the third set of data of Table 2, 30 modes of Mathieu RCWA algorithm (M(R1,R3),SV(R2)) were used to compute normalized power results using $N_\ell = 150, 300, 600, 1200, 2400$ layers and the number of SV harmonics was taken to be $N_{SV} = 54$ in all cases except the one where it was taken to be $N_{SV} = 107$. As can be seen, for a given number of layers N_ℓ, power conservation at the interfaces $u = u_a^-$, $u = u_a^+$, $u = u_b^-$, and $u = u_b^+$ is obeyed to a high degree of accuracy (5 or 6 place accuracy), but for different numbers of layers N_ℓ, slightly different values of the normalized power are seen. It is also observed as the number of layers is increased, that the normalized power changes value by a smaller and smaller amount, and thus one can conclude that convergence of the Mathieu RCWA algorithm to the exact answer is occurring. The normalized power data for the 1200 layer, 30 mode case, was calculated using both $N_{SV} = 54$ and $N_{SV} = 107$ SV harmonics. As can be seen very close numerical results for these two cases were observed. From this we conclude that $N_{SV} = 54$ SV harmonics was sufficient for accurate numerical results. As in Table 1 (uniform profile Reg. R2 case (or homogeneous case)), we see overall, that the number of layers N_ℓ is the most sensitive parameter as to establishing an accurate solution.

4. SUMMARY AND CONCLUSION

In this paper numerical convergence results and validation results for the RCWA algorithm has been provided for two numerical examples, a homogeneous one which corresponded to a uniform material profile in Reg. R2 and an inhomogeneous one which corresponded a dielectric step profile in Reg. R2.

Numerical convergence and validation results for the homogenous case were displayed in Table 1 which presented the normalized power which occurred in the elliptical system when different sets of expansion functions were used, when different numbers of modes were and when a different number of layers were used. It was found that as the number of layers and modes were increased that the Hankel-Bessel or Mathieu RCWA algorithms converged to the matrix solution which resulted when either Mathieu expansion modes were used in all regions M(R1,R2,R3) or when Hankel Bessel functions were used in Regs. R1 and R3 and Mathieu modes were used in Reg. R2. Numerical convergence and validation results were also displayed in Figs. 2–6 where RCWA electric and magnetic fields at the region interfaces were shown using different expansion modes and different numbers of layers.

Numerical convergence and validation results for the inhomogeneous case were displayed in Table 2 which presented the normalized power data which occurred in the elliptical system when different sets of expansion functions were used to form the RCWA algorithm, when different numbers of modes were used, when a different number of layers were used, and when different number of SV harmonics were used. It was found that as the number of layers, modes, and SV harmonics were increased, that the Hankel-Bessel or Mathieu algorithms numerical results changed less and less, and thus converged to a final solution.

In both the homogeneous and inhomogeneous examples, power conservation at the different interfaces was observed when a sufficient number of modes were used in the solution. In observing the convergence data of Tables 1 and 2, and Figs. 2–6, the author feels that the number of layers used was an important parameter as to establishing an accurate Hankel-Bessel or Mathieu RCWA solution. It was also found for the step profile numerical example tested, that the number of modes used in the RCWA algorithms needed to exceed a critical minimum value (in Table 2 about 18 to 20 modes) in order to obtain meaningful and accurate results. For 14 to 16 modes for example, highly incorrect and ill-conditioned numerical results occurred. It was further found that once this critical minimum of modes was exceeded, that the RCWA converged quickly to an accurate solution.

In conclusion the author feels that the Hankel-Bessel and Mathieu RCWA algorithms as presented have correctly solved the numerical examples which have been presented. The author bases this conclusion on the facts that power conservation, validation by independent methods, and the demonstration of proper EM field boundary matching has occurred. The author believes that the Hankel-Bessel and Mathieu RCWA algorithms can provide solutions to more numerically challenging, inhomogeneous examples than have been presented herein.

REFERENCES

1. Jarem, J. M., "Rigorous coupled wave analysis of radially and azimuthally-inhomogeneous, elliptical, cylindrical systems," *Progress In Electromagnetics Research,* PIER 34, 89–115, 2001.

2. Moharam, M. G. and T. K. Gaylord, "Rigorous coupled-wave analysis of planar grating diffraction," *J. Opt. Soc. Amer.,* Vol. 71, 811–818, 1981.

3. Moharam, M. G. and T. K. Gaylord, "Diffraction analysis of

dielectric surface-relief gratings," *J. Opt. Soc. Amer.,* Vol. 72, 1385–1392, 1982.

4. Jarem, J. M., "Rigorous coupled wave theory solution of phi-periodic circular cylindrical dielectric systems," *Journal of Electromagnetic Waves and Applications,* Vol. 11, 197–213, 1997.

5. Jarem, J. M., "Rigorous coupled wave theory of anisotropic, azimuthally-inhomogeneous, cylindrical systems," *Progress in Electromagnetics Research,* PIER 19, Chap. 4, 109–127, 1998.

6. Jarem, J. M. and P. P. Banerjee, "Bioelectromagnetics: A rigorous coupled wave analysis of cylindrical biological tissue," *Proceedings of the International Conference on Mathematics and Engineering Techniques in Medicine and Biological Sciences, (METMBS'00),* F. Valafar (Ed.), 467–472, Vol. II, Las Vegas, Nev., June 26–29, 2000.

7. Jarem, J. M., "Rigorous coupled-wave-theory analysis of dipole scattering from a three-dimensional, inhomogeneous, spherical dielectric and permeable system," *IEEE Microwave Theory and Techniques,* Vol. 45, No. 8, 1193–1203, Aug. 1997.

8. Jarem, J. M. and P. P. Banerjee, *Computational Methods for Electromagnetic and Optical Systems,* Marcel Dekker, Inc. 2000.

9. Bowman, J. J, T. B. Senior, and P. L. E. Uslenghi, *Electromagnetic and Acoustic Scattering by Simple Shapes,* Chap. 3, "The Elliptic Cylinder", 129–180, Hemisphere Publishing Corp., New York, N.Y., revised printing, 1987.

10. Sebak, A. R., "Scattering from dielectric-coated impedance elliptic cylinder," *IEEE Transactions on Antennas and Propagation,* Vol. 48, No. 10, 1574–1580, Oct. 2000.

11. Abramowitz, M. and I. Stegum, *Handbook of Mathematical Functions,* Chap. 20, "Mathieu Functions", Dover publications, New York, N.Y., 1972.

12. Zhang, S. and J. Jin, "FORTRAN routines for computation of special functions," Programs: "MTU12,MTU0,FCOEF,CVF, CVA2" at Web Site http://iris-lee3.ece.uiuc.edu/j̃jin/routines/ routines.html, Mar. 8,01. (Programs associated with the book Computation of Special Functions, John Wiley and Sons. Inc.)